Wirestam, R and Ståhlberg, F

"Wavelet-based noise reduction for improved deconvolution of
time-series data in dynamic susceptibility-contrast MRI."

MAGMA. 2005 Jul;18(3):113-8.

Publisher: Springer.

Alternative location: http://dx.doi.org/10.1007/s10334-005-0102-z

Wavelet-based noise reduction for improved deconvolution of time-series data in dynamic susceptibility contrast MRI

R. Wirestam[1] and F. Ståhlberg[1,2]

1) Department of Medical Radiation Physics, Lund University Hospital, Lund, Sweden
2) Department of Diagnostic Radiology, Lund University Hospital, Lund, Sweden

Correspondence to:

Ronnie Wirestam, Ph.D.
Dept. of Medical Radiation Physics
Lund University Hospital
SE-22185 Lund, Sweden

Fax: +46 46 178540
Email: ronnie.wirestam@radfys.lu.se

ABSTRACT

Objective: Dynamic susceptibility contrast (DSC) MRI requires deconvolution for retrieving the tissue residue function R(t) and the cerebral blood flow (CBF). In this study, deconvolution of time-series data was performed by wavelet-transform based denoising combined with the Fourier transform (FT). Materials and Methods: Traditional FT-based deconvolution of noisy data requires frequency-domain filtering, often leading to excessive smoothing of the recovered signal. In the present approach, only a low degree of regularisation was employed while the major noise reduction was accomplished by wavelet transformation of data and Wiener-like filtering in the wavelet space. After inverse wavelet transform, the estimate of CBF·R(t) was obtained. DSC-MRI signal-versus-time curves (signal-to-noise ratios 40 and 100) were simulated, corresponding to CBF values in the range 10-60 ml/(min 100g). Three shapes of the tissue residue function were investigated. The technique was also applied to 6 volunteers. Results: Simulations showed CBF estimates with acceptable accuracy and precision, as well as independence of any time shift between the arterial input function and the tissue concentration curve. The grey-matter to white-matter CBF ratio in volunteers was 2.4±0.2. Conclusion: The proposed wavelet/FT deconvolution is robust and can be implemented into existing perfusion software. CBF maps from healthy volunteers showed high quality.

Key words: Deconvolution, dynamic susceptibility contrast, magnetic resonance imaging, perfusion, cerebral blood flow, wavelets, noise

INTRODUCTION

Accurate and robust deconvolution algorithms are essential for obtaining reliable regional cerebral blood flow (CBF) estimates by use of an intravascular tracer. In dynamic susceptibility-contrast (DSC) MRI for assessment of brain perfusion (1), singular value decomposition (SVD) is a common tool for solving the convolution integral in matrix form, in order to obtain the impulse residue function R(t) of the tissue of interest from the tissue concentration time curve C(t) and the arterial input function AIF or $C_{art}(t)$ (2). The initial implementations of the SVD deconvolution algorithm (denoted 'standard SVD' in this report) are sensitive to even a modest time delay between the two functions involved, i.e. between the measured arterial input function and the corresponding tissue concentration time curve (3). Wu et al. (4) and Smith et al. (5) have recently presented modified SVD-based algorithms, insensitive to arterial-tissue delay.

Alternative deconvolution techniques have been introduced for use in DSC-MRI. For example, Østergaard et al. investigated a number of approaches, both model-dependent and model-independent, in a simulation study (1). Examples of other recent DSC-MRI deconvolution approaches are likelihood-based algorithms, such as iteration schemes for maximum likelihood expectation maximisation (6) and estimation of the impulse residue function as the mean value of an optimised joint Gaussian distribution (7). Furthermore, the classical filtered Fourier-transform (FT) deconvolution was employed by Rempp et al. (8), and has later been compared with SVD-based techniques using experimental DSC-MRI data (9, 10).

Deconvolution based on division in the frequency domain, after Fourier transform of C(t) and $C_{art}(t)$, has the advantage of being insensitive to possible time delays between the two functions. On the other hand, the conventional FT-based deconvolution requires the application of a filter (e.g. the Wiener filter) in the frequency domain in order to suppress the effects of noise. Unfortunately, such filters inevitably result in a smoothing of the recovered function and a corresponding suboptimal representation of edges. In DSC-MRI perfusion measurements, the CBF is theoretically given by the initial value of a continuously decreasing tissue residue function, i.e. by a value that corresponds to the edge of a function. In the present study, a hybrid deconvolution approach, combining a Fourier-domain regularisation with wavelet-based denoising (11), is proposed for CBF calculation in DSC-MRI.

METHOD

Theory of DSC-MRI perfusion measurements

Briefly, the assumed relationship between the measured signal S and the concentration C_m is given by Eq. 1 (1):

$$C_m(t) = -\frac{1}{k\,TE}\ln\left[\frac{S(t)}{S_0}\right] \quad \Leftrightarrow \quad S(t) = S_0 e^{-kC_m(t)TE} \qquad [1]$$

where k is a proportionality constant, t is time, TE is echo time and S_0 is the baseline signal. A correction factor k_H (set to 0.705 ml/g in the present study), including brain density and the haematocrit values in large and small vessels, is normally applied, i.e. $C(t)=k_H \cdot C_m(t)$ (8). The CBF is then defined by the convolution in Eq. 2:

$$C(t) = CBF\left[R(t) \otimes C_{art}(t)\right] \qquad [2]$$

Deconvolution strategy

In order to obtain a convolution filter with normalised area, rescaled concentration parameters were introduced by dividing the tissue concentration C(t) as well as the arterial concentration $C_{art}(t)$ with the area under the arterial concentration curve, i.e.

$$C_s(t) = \frac{C(t)}{\int_0^\infty C_{art}(t)dt} \qquad [3a]$$

$$AIF(t) = \frac{C_{art}(t)}{\int_0^\infty C_{art}(t)dt} \qquad [3b]$$

Furthermore, the scaled tissue residue function was defined as $R_s(t)=CBF \cdot R(t)$, and the relationship between the measured tissue concentration, the arterial concentration and the tissue residue function is given by the convolution integral:

$$C_s(t) = \int_0^t AIF(\tau)R_s(t-\tau)d\tau \qquad [4]$$

Basic FT-based deconvolution, with notations from DSC-MRI, can be mathematically described as follows:

$$R_s(t) = FT^{-1}\left[\frac{FT\left[C_s(t)\right]}{FT\left[AIF(t)\right]}\right] \qquad [5]$$

In the presence of noise, frequency-domain, low-pass filtering is normally applied, in order to obtain a reasonable estimate of the scaled tissue residue function, denoted $[R_s(t)]_\alpha$. A typical representation of such a filter is given by Eq. 6:

$$\left[\mathrm{R_s(t)}\right]_\alpha = FT^{-1}\left[\frac{\mathrm{G}_\alpha(\mathrm{f})\cdot FT\left[\mathrm{C_s(t)}\right]}{FT\left[\mathrm{AIF(t)}\right]}\right] \text{ where } \mathrm{G}_\alpha(\mathrm{f}) = \frac{|FT[\mathrm{AIF(t)}]|^2}{\left|FT[\mathrm{AIF(t)}]\right|^2 + \frac{\mathrm{N}\alpha\sigma^2}{\left|FT\left[\mathrm{R_s(t)}\right]\right|^2}} \quad [6]$$

$|FT[R_s(t)]|^2$ is an approximation of the power spectral density of the input signal. Furthermore, σ^2 is the variance of the noise and α is the regularisation parameter that controls the trade-off between noise suppression and signal distortion. The factor N, i.e. the number of data points used in the discrete Fourier transform, is included due to the general convention that $\sum_k \left|FT\left[C_s\right](f_k)\right|^2 = N\sum_k \left|C_s(k)\right|^2$. When α is large, the shape of R(t) becomes distorted, i.e. R(t) is smoothed and its edges become less sharp, and, on the other hand, if α=0 the deconvolution is severely hampered by noise. The Wiener filter corresponds to the setting of α=1.

The use of Eq. 6 requires knowledge about $R_s(t)$ for determination of $|FT[R_s(t)]|^2$, and this function is obviously unknown in practise. In the present study, a Tikhonov regularised FT-based estimate, denoted $[R_s(t)]_T$, obtained using a constant regularisation parameter T, was used as an approximation:

$$\left[\mathrm{R_s(t)}\right]_T = FT^{-1}\left[\frac{\mathrm{G}_T(\mathrm{f})\cdot FT\left[\mathrm{C_s(t)}\right]}{FT\left[\mathrm{AIF(t)}\right]}\right] \text{ where } \mathrm{G_T(f)} = \frac{|FT[\mathrm{AIF(t)}]|^2}{\left|FT[\mathrm{AIF(t)}]\right|^2 + T} \quad [7]$$

Hence, by applying the initial approximation $R_s(t)\approx[R_s(t)]_T$ to Eq. 6, an approximation to $[R_s(t)]_\alpha$ was obtained:

$$\left[\mathrm{R_s(t)}\right]_\alpha = FT^{-1}\left[\frac{\mathrm{G}_\alpha(\mathrm{f})\cdot FT\left[\mathrm{C_s(t)}\right]}{FT\left[\mathrm{AIF(t)}\right]}\right] \text{ where } \mathrm{G}_\alpha(\mathrm{f}) = \frac{|FT[\mathrm{AIF(t)}]|^2}{\left|FT[\mathrm{AIF(t)}]\right|^2 + \frac{\mathrm{N}\alpha\sigma^2}{\left|FT\left[\left[\mathrm{R_s(t)}\right]_\mathrm{T}\right]\right|^2}} \quad [8]$$

In the present study, a low α value was employed, and the major noise reduction was accomplished by discrete wavelet transformation of $[R_s(t)]_\alpha$, followed by Wiener-like filtering in the wavelet space (see Eq. 10). However, the calculation of the shrinkage factors δ_j requires knowledge of the wavelet coefficients w_j of the true signal $R_s(t)$, so the application of Eq. 10 was proceeded by a moderate hard thresholding, i.e. the wavelet coefficient was set to zero if $|w_j|$ was smaller than a certain threshold value (Eq. 9):

$$w_j' = \delta_j' w_j, \text{ where } \delta_j' = \begin{cases} 1 & if\ |w_j| > \rho\sigma \\ 0 & if\ |w_j| \le \rho\sigma \end{cases} \quad [9]$$

where ρ is a threshold factor. Thereafter, the Wiener-like filtering was applied to shrink each wavelet coefficient w_j' by a factor δ_j, according to Eq. 10:

$$w_j'' = \delta_j w_j', \text{ where } \delta_j = \frac{|w_j'|^2}{|w_j'|^2 + \sigma^2} \quad [10]$$

After inverse wavelet transform, the final estimate of $R_s(t)$ was attained, and the maximal value of the $R_s(t)$ estimate was assumed to represent CBF. The wavelet used was the Daubechies family wavelet of grade 2, and an approximation of the noise variance σ^2 was obtained as the variance of the finest scale wavelet coefficients.

The computer program for deconvolution of DSC-MRI data using the above concept was designed in Interactive Data Language (IDL 6.0, Research Systems Inc.), using the features of the *IDL Wavelet Toolbox* for the discrete wavelet transform.

Simulations

The simulation procedure was designed to facilitate comparison with previously published investigations of deconvolution techniques applied to DSC-MRI. Realistic DSC-MRI data (64 data points with a temporal resolution of 1.0 s) for artery as well as for tissue were simulated, corresponding to a constant CBV of 4 ml/100g and CBF values ranging from 10 to 60 ml/(min 100g). The arterial concentration curve was defined by $C_{art}(t)=k_{art}(t-t_0)^3\exp(-(t-t_0)/1.5\text{ s})$ $(t>t_0)$, where k_{art} is a constant adjusted to give a reasonable signal loss during the simulated contrast-agent passage (2, 12). A recirculation effect was introduced by adding a downscaled and time-shifted copy of the above function convolved with an exponential function with time constant 30 s (12).

Three different shapes of the tissue residue function R(t) were investigated, namely exponential, triangular and box-shaped. The explicit mathematical definitions of these functions can be found in the paper by Murase et al. (12). In order to obtain the corresponding tissue concentration curves, the tissue residue functions were convolved with the arterial concentration curve.

In the next step, arterial and tissue signal curves were generated using Eq. 1, using S_0 values of 200 and 600 for tissue and artery, respectively. Due to the large tracer concentration differences between artery and tissue, it is difficult to obtain a reasonably large signal drop in tissue without at the same time saturating the arterial signal (13). One solution is to set a shorter TE for a slice through a brain-feeding artery and a longer echo-time for the tissue slices (14, 15), and this approach was assumed in the present simulations with TE_{art}=0.013 s and TE_{tissue}=0.055 s. Random noise from a Gaussian distribution with standard deviation σ was added to the tissue signal curve to yield a desired signal-to-noise ratio (SNR = S_0/σ) of the tissue baseline signal. The arterial noise distribution was modified to be Rician, since arterial signal might drop to very low levels. The main part of the simulations was carried out at SNR=40, assumed to approximately represent a "low-SNR situation" in

DSC-MRI. To assure that the proposed method is not severely dependent on SNR, a "high-SNR situation" was also investigated (with the same settings of T, α and ρ). The selected SNR levels were based on limited experimental DSC-MRI data from gradient-echo (GRE) echo-planar imaging (EPI) with TE=55 ms at 1.5 T (SNR of the order of 40) and TE=21 ms at 3.0 T (SNR of the order of 100). Note that these experimental data were used only to roughly establish the baseline SNR in tissue.

After noise addition, the noisy concentration curves for artery and tissue were calculated according to Eq. 1. The arterial and tissue data arrays were then doubled, i.e., extended to 128 positions. In this added part of the array, concentration data were extrapolated gradually towards zero, according to the formula suggested by Gobbel & Fike (16), in order to avoid extreme high-frequency oscillations at the end of the deconvolved curve. CBF was then calculated according to the theory outlined above. In order to optimise the combination of T, α and ρ, estimates of the CBF error were introduced in the simulations. First, the error $|CBF_{true}-\max[[R_s(t)]_T]|/CBF_{true}$ (averaged over all investigated CBF values and all shapes of the tissue residue function) was calculated for a number of T values. By using the optimal T value, a reasonable combination of α and ρ was determined in a similar way, by finding the combination of α and ρ that minimised the error $|CBF_{true}- CBF_{simulated}|/CBF_{true}$ (averaged over all investigated CBF values and all shapes of the tissue residue function). $CBF_{simulated}$ denotes the final estimate of CBF in the simulations.

Keeping in mind that previously presented deconvolution methods (e.g., 2) have shown pronounced sensitivity to any time delay between arterial and tissue concentration curves (at short MTT), calculations of CBF were also carried out with tissue-curve time shifts of up to ±3 seconds. In the simulations of time-delay effects, the true CBF value was 60 ml/(min 100g), corresponding to MTT=4 s (i.e. the shortest MTT investigated in this study).

Experiments

The technique was also applied to *in vivo* data from six healthy volunteers, 3 males and 3 females, in the age range 21 – 26 years (average age 23 years). Written informed consent was obtained before the DSC-MRI experiment, and the study was approved by the local ethics committee. Each of the volunteers received 0.2 mmol/kg bodyweight of a gadobutrol contrast agent (Gadovist® 1.0, Schering AG, Berlin, Germany). The contrast agent was administered into a peripheral arm vein using a power injector at a rate of 5 ml/s, followed by a 40 ml saline flush with the same injection rate. Injection was started 18 s after the start of the perfusion imaging sequence. DSC-MRI was carried out using a 3 T head scanner (Siemens Magnetom Allegra), employing a GRE-EPI pulse sequence with echo time 21 ms, slice thickness 5 mm, interslice gap 1.5 mm, field of view 210×210 mm^2 and image matrix 128×128. Twenty slices with a total of 60 images per slice were recorded, with a temporal resolution of 1.5 s over a period of 90 seconds. Oblique transversal-to-coronal slices were positioned so that the second lowest slice passed through the pons/medulla junction and the root of the nose.

Acquired signal data were post-processed according to the procedures described in the above sections. The AIF was typically recorded from an artery in the Sylvian fissure region. Similarly to the simulated data, arterial and tissue data arrays were extended to 128 positions and concentration data were extrapolated gradually towards zero (16). Relative CBF maps were calculated using the proposed wavelet/FT-based deconvolution concept with T=0.015, α=0.1 and ρ=4.0. Ratios of CBF in grey matter to CBF in white matter were calculated from relative CBF values taken from regions of interest in thalamus grey matter (GM) and frontal white matter (WM).

RESULTS

In Figure 1a, the error estimate $|CBF_{true}-\max[[R_s(t)]_T]|/CBF_{true}$ (averaged over all investigated CBF values and all shapes of the tissue residue function) is given as a function of T. From this plot, the optimal value of T=0.015 was obtained. Figure 1b shows the CBF error $|CBF_{true}- CBF_{simulated}|/CBF_{true}$ (averaged over all investigated CBF values and all shapes of the tissue residue function) for different combinations of α and ρ. From several reasonable combinations of α and ρ, all corresponding to a low CBF error, the combination α=0.1 and ρ=4.0 was selected for use in the subsequent applications of the wavelet/FT deconvolution method.

Figures 2a and 2b show results from the simulation study, i.e. estimated CBF versus true CBF obtained at SNR=40 and SNR=100, respectively, using the wavelet/FT-based deconvolution with T=0.015, α=0.1 and ρ=4.0. Figure 3 illustrates the ratio of simulated CBF to true CBF (at SNR=40) as a function of the delay time between the AIF and the tissue concentration curve; the true CBF value was 60 ml/(min 100g), corresponding to MTT=4 s.

The experimentally obtained GM-to-WM CBF ratio was 2.44±0.13 (mean±SD), and the individual results from the six healthy volunteers are given in Table 1. Figure 4 displays relative CBF maps corresponding to three centrally located slices, calculated by the wavelet/FT deconvolution technique.

DISCUSSION

The discrete wavelet transform is a powerful tool for reduction of noise in time series data. In the present project, a relatively simple method was implemented by use of the *Wavelet Toolkit* available in IDL and incorporated into a well-established FT-based deconvolution strategy. Compared with conventional FT-based deconvolution of noisy data (2), the presently proposed algorithm appears to provide considerably higher accuracy at high CBF (i.e. short MTT), due to the minimal filtering required. Furthermore, the wavelet/FT deconvolution approach is computationally not too demanding and the results are insensitive to any time delays occurring between the site of the measured AIF and the concentration curve of the tissue of interest.

The optimisations of T, α and ρ were carried out at SNR=40, but Figure 2 indicates that no pronounced SNR dependence of the estimated mean values is at hand when SNR is increased. The standard deviations of the CBF estimates were, as expected, reduced at SNR=100. It might be worthwhile to further optimise T, α and ρ for other appropriate SNR levels, but this was beyond the scope of the current phase of the project. The results of the present investigation indicate that the wavelet/FT deconvolution technique provides an acceptable accuracy over the entire range of CBF values. The tendency towards a slight overestimation at low CBF (longer MTT) and an underestimation for the exponential residue function at high CBF (short MTT) is typical also for the SVD techniques, as illustrated by Wu et al. (4) and Andersen et al. (7). The standard deviation (SD) of the simulated wavelet/FT CBF estimates appeared to be slightly higher than for the standard SVD technique, as indicated by graphs presented by Østergaard et al. (2) and Andersen et al. (7). However, Andersen et al. (7) claimed that the low standard deviations often seen when standard SVD is employed can, to a significant extent, be the result of an inherent erroneous behaviour of the SVD technique. The method based on retrieving the mean value of an optimised joint Gaussian distribution (7) shows excellent performance, but is computationally demanding and very time consuming. The algorithm proposed by Vonken et al. (6) displays, at a given number of iterations, underestimated CBF values at short MTT when a time delay between the arterial input curve and the tissue response is introduced. This effect can, however, be minimised by employing a larger number of iterations.

Finally, the *in vivo* example (Fig. 4) shows that the wavelet/FT algorithm provides CBF maps of high quality. The observed GM-to-WM CBF ratio of 2.44 is in accordance with previously presented results obtained by other medical imaging modalities. For example, the PET investigation by Leenders et al. (17) showed an average GM-to-WM ratio of 2.46. The Tc-99m-HMPAO SPECT study by Wirestam et al. (18) resulted in a somewhat lower ratio of 2.24, but it should be remembered that the subjects in the SPECT study were considerably older (average age 66 years).

In conclusion, the proposed deconvolution technique is an interesting alternative to previously presented methods. The accuracy and precision of the wavelet/FT-based

CBF estimates are comparable with the state-of-the art SVD algorithms, the results are insensitive to any time shift of the measured AIF compared with the true AIF, the calculation procedure is typically faster than for likelihood-based methods, and the required mathematical algorithms can easily be implemented into existing perfusion software (e.g., 19).

ACKNOWLEDGEMENTS

This project was supported by the Crafoord Foundation, the Thorsten and Elsa Segerfalk Foundation and the Swedish Research Council (grant no. 13514).

REFERENCES

1. Rosen BR, Belliveau JW, Vevea JM, Brady TJ (1990) Perfusion imaging with NMR contrast agents. Magn Reson Med 14:249-265.

2. Østergaard L, Weisskoff RM, Chesler DA, Gyldensted C, Rosen BR (1996) High resolution measurement of cerebral blood flow using intravascular tracer bolus passages. Part I: Mathematical approach and statistical analysis. Magn Reson Med 36:715-725.

3. Calamante F, Gadian DG, Connelly A (2000) Delay and dispersion effects in dynamic sucseptibily contrast MRI: Simulations using singular value decomposition. Magn Reson Med 44:466-473.

4. Wu O, Østergaard L, Weisskoff RM, Benner T, Rosen BR, Sorensen AG (2003) Tracer arrival timing-insensitive technique for estimating flow in MR perfusion-weighted imaging using singular value decomposition with a block-circulant deconvolution matrix. Magn Reson Med 50:164-174.

5. Smith MR, Lu H, Trochet S, Frayne R (2004) Removing the effect of SVD algorithmic artifacts present in quantitative MR perfusion studies. Magn Reson Med 51:631-634.

6. Vonken EP, Beekman FJ, Bakker CJ, Viergever MA (1999) Maximum likelihood estimation of cerebral blood flow in dynamic susceptibility contrast MRI. Magn Reson Med 41:343-350.

7. Andersen IK, Szymkowiak A, Rasmussen CE, Hanson LG, Marstrand JR, Larsson HBW, Hansen LK (2002) Perfusion quantification using gaussian process deconvolution. Magn Reson Med 48:351-361.

8. Rempp KA, Brix G, Wenz F, Becker CR, Guckel F, Lorenz WJ (1994) Quantification of regional cerebral blood flow and volume with dynamic susceptibility contrast-enhanced MR imaging. Radiology 193:637-641.

9. Wirestam R, Andersson L, Østergaard L, Bolling M, Aunola J-P, Lindgren A, Geijer B, Holtås S, Ståhlberg F (2000) Assessment of regional cerebral blood flow by dynamic susceptibility contrast MRI using different deconvolution techniques. Magn Reson Med 43:691-700.

10. Smith AM, Grandin CB, Duprez T, Mataigne F, Cosnard G (2000) Whole brain quantitative CBF and CBV measurements using MRI bolus tracking: comparison of methodologies. Magn Reson Med 43:559-564.

11. Neelamani R, Hyeokho Choi, Baraniuk R (2004) ForWaRD: Fourier-wavelet regularized deconvolution for ill-conditioned systems. IEEE Trans. Signal Processing 52:418-433.

12. Murase K, Shinohara M, Yamazaki Y (2001) Accuracy of deconvolution analysis based on singular value decomposition for quantification of cerebral blood flow using dynamic susceptibility contrast-enhanced magnetic resonance imaging. Phys Med Biol 46:3147-3159.

13. Ellinger R, Kremser C, Schocke MF, Kolbitsch C, Griebel J, Felber SR, Aichner FT (2000) The impact of peak saturation of the arterial input function on quantitative evaluation of dynamic susceptibility contrast-enhanced MR studies. J Comput Assist Tomogr 24:942 -948.

14. Perman WH, Gado MH, Larson KB, Perlmutter JS (1992) Simultaneous MR acquisition of arterial and brain signal-time curves. Magn Reson Med 28:74-83.

15. Vonken EJ, van Osch MJP, Bakker CJG, Viergever MA (1999) Measurement of cerebral perfusion with dual-echo mutli-slice quantitative dynamic susceptibility contrast MRI. J Magn Reson Imaging 10:109–117.

16. Gobbel GT, Fike JR (1994) A deconvolution method for evaluating indicator-dilution curves. Phys Med Biol 39:1833-1854.

17. Leenders KL, Perani D, Lammertsma AA, Heather JD, Buckingham P, Healy MJR, Gibbs JM, Wise RJS, Hatazawa J, Herold S, Beaney RP, Brooks DJ, Spinks T, Rhodes C, Frackowiak RSJ, Jones T (1990) Cerebral blood flow, blood volume and oxygen utilization. Brain 113:27-47.

18. Wirestam R, Ryding E, Lindgren A, Geijer B, Østergaard L, Andersson L, Holtås S, Ståhlberg F (2000) Regional cerebral blood flow distributions in normal volunteers: Dynamic susceptibility contrast MRI compared with ^{99m}Tc-HMPAO SPECT. J Comput Assist Tomogr 24:526-530.

19. Thilmann O (2004) LUPE: An extensible modular framework for evaluation of DSC-acquired perfusion images. Proc. of the 21st Annual Meeting of the ESMRMB. MAGMA 16 (electronic suppl. 1):537.

Table 1. Ratios of CBF in thalamus grey matter to CBF in frontal white matter obtained in six healthy volunteers.

Volunteer #	CBF_{GM}/CBF_{WM}
1	2.66
2	2.34
3	2.28
4	2.51
5	2.41
6	2.46
mean±SD	2.44±0.13

FIGURE LEGENDS

Figure 1a:

The error in the simulated, preliminary CBF estimate (see Eq. 7) as a function of the regularisation parameter T at SNR=40. Each data point corresponds to the mean value of 500 simulations. The displayed uncertainties were calculated by standard error-propagation theory using the observed standard deviations of the simulated parameter $\max[[R_s(t)]_T]$ as input.

Figure 1b:

Surface plot of the error in the simulated CBF estimate for different combinations of α and ρ at SNR=40. Each data point corresponds to the mean value of 200 simulations.

Figure 2:

Simulated CBF estimates versus true CBF for three different shapes of the tissue residue function (exponential, triangular and box-shaped). The simulated CBF values were obtained by the wavelet/FT deconvolution technique assuming a baseline tissue signal-to-noise ratio of **(a)** 40 and **(b)** 100. For each data point, the simulations were repeated 1000 times and the error bars correspond to ±1 SD.

Figure 3:

The ratio of simulated CBF to true CBF as a function of the time shift between the AIF curve and the tissue concentration curve. The simulation was carried out with true CBF=60 ml/(min 100g), CBV=4.0 ml/100g, MTT=4.0 s and SNR=40. Negative time shifts correspond to cases when the tissue concentration curve preceded the AIF. For each data point, the simulations were repeated 1000 times.

Figure 4:

Relative CBF maps from a healthy volunteer, calculated using the proposed wavelet/FT deconvolution algorithm.

Figure 1a

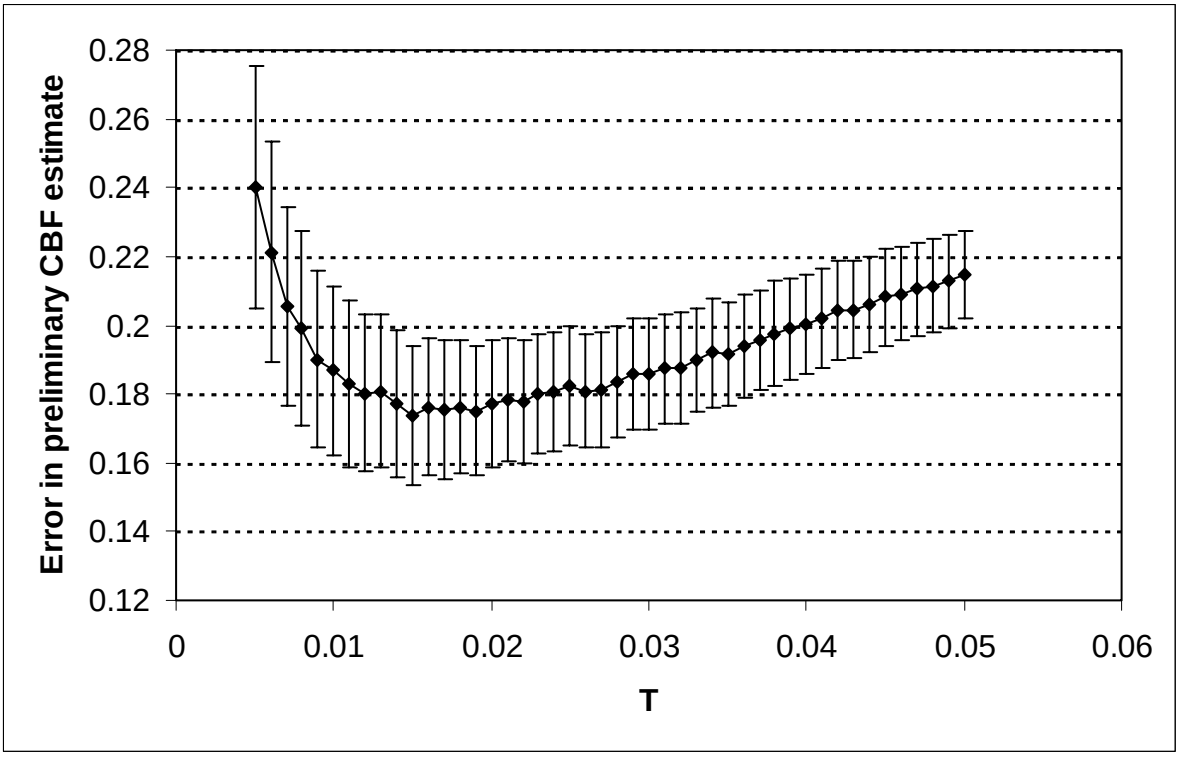
Error in preliminary CBF estimate
0.28
0.26
0.24
0.22
0.2
0.18
0.16
0.14
0.12
0
0.01
0.02
0.03
0.04
0.05
0.06
T

Figure 1b

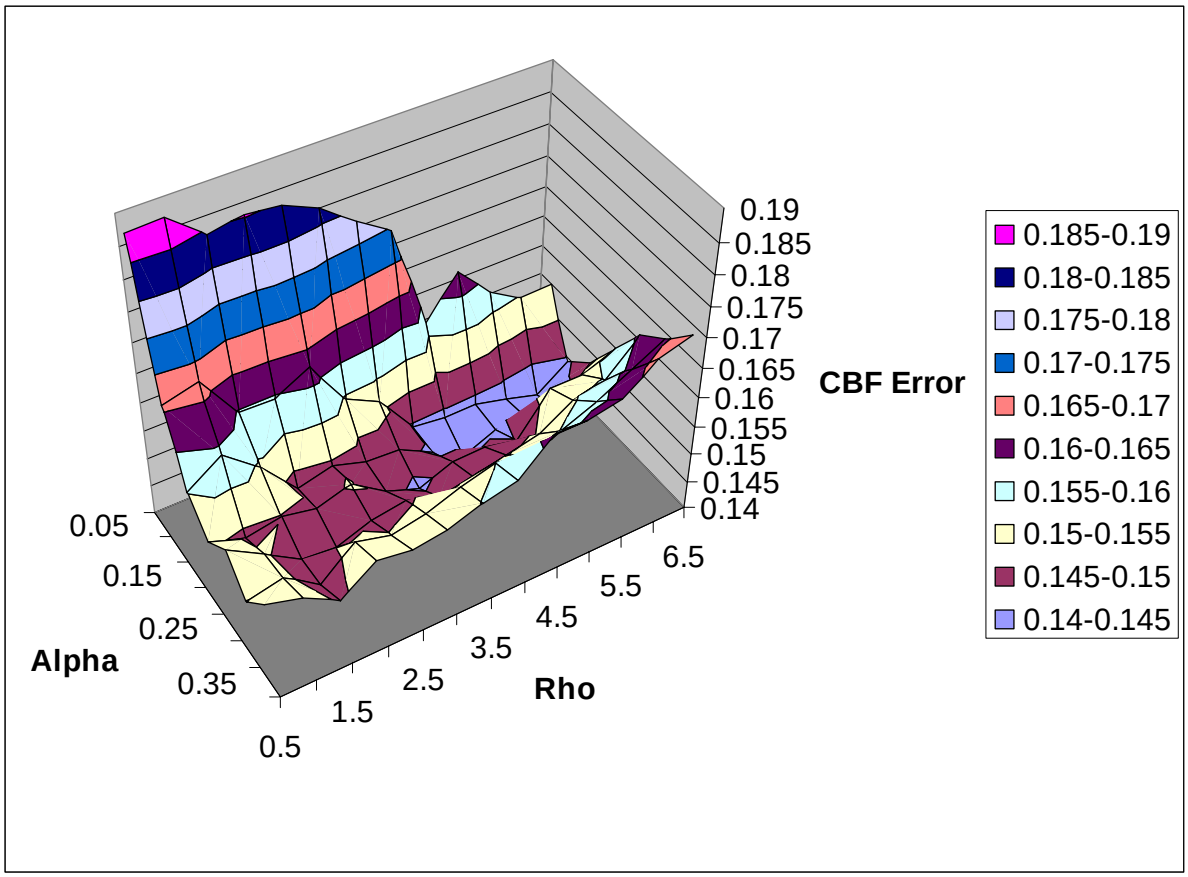
0.19
0.185
0.18
0.175
0.17
0.165
0.16
0.155
0.15
0.145
0.14
CBF Error
0.185-0.19
0.18-0.185
0.175-0.18
0.17-0.175
0.165-0.17
0.16-0.165
0.155-0.16
0.15-0.155
0.145-0.15
0.14-0.145
0.05
0.15
0.25
0.35
Alpha
0.5
1.5
2.5
3.5
4.5
5.5
6.5
Rho

Figure 2a

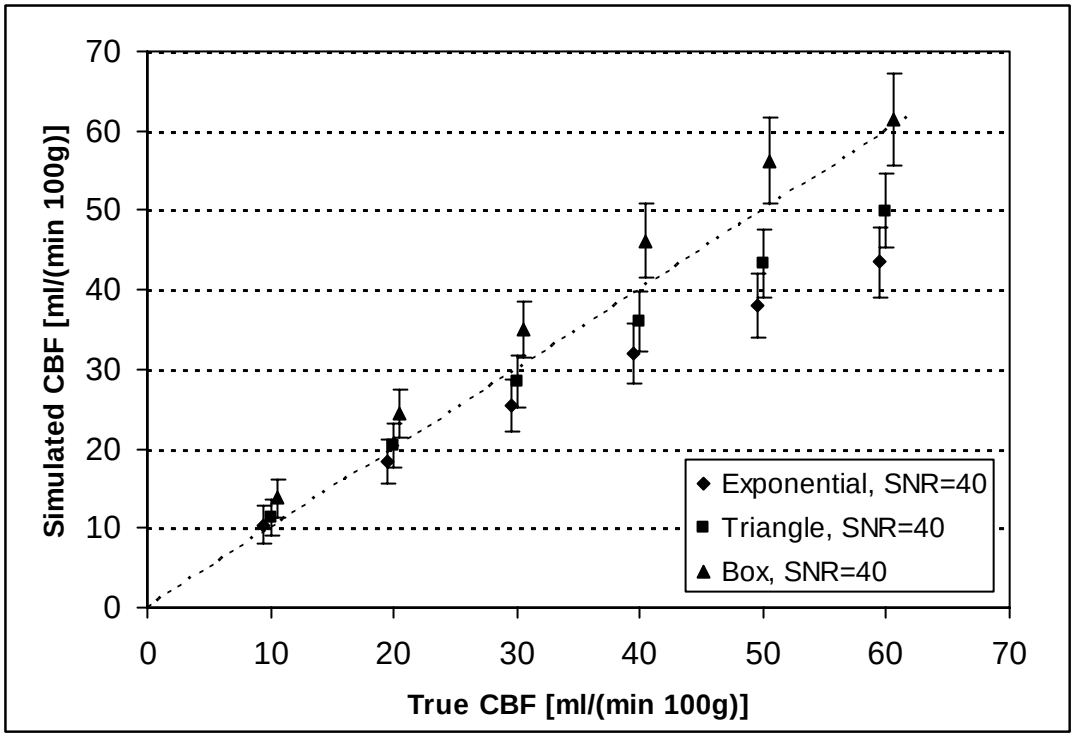
Simulated CBF [ml/(min 100g)]
True CBF [ml/(min 100g)]
0
10
20
30
40
50
60
70
Exponential, SNR=40
Triangle, SNR=40
Box, SNR=40

Figure 2b

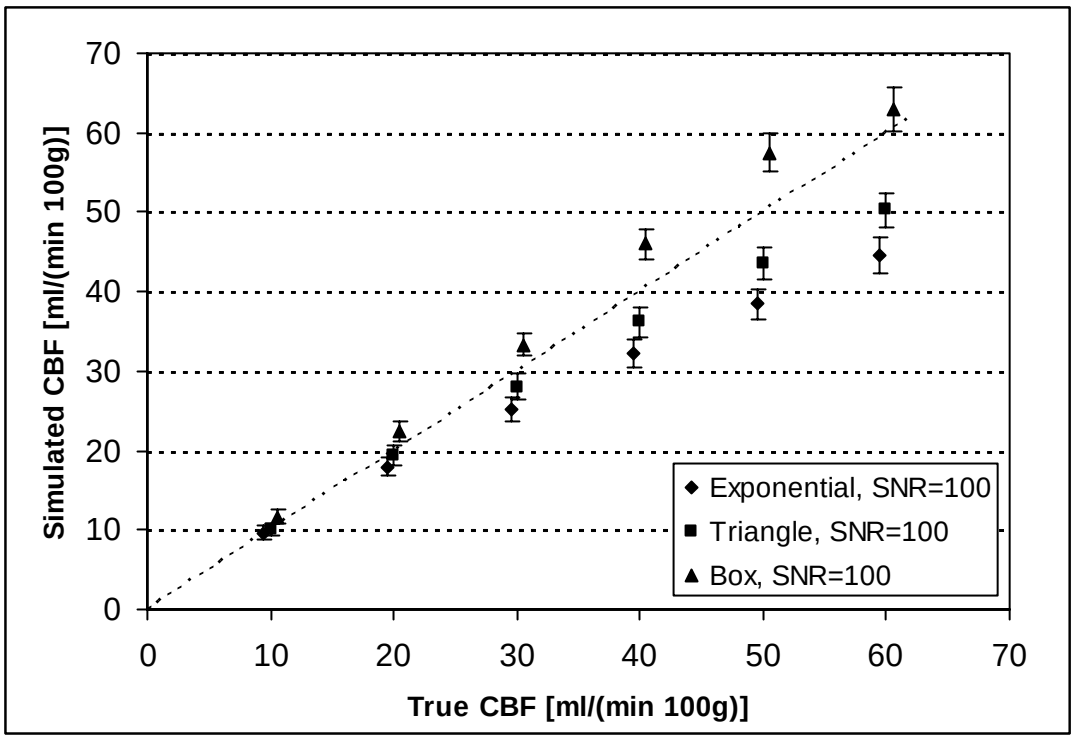
Simulated CBF [ml/(min 100g)]
True CBF [ml/(min 100g)]
0
10
20
30
40
50
60
70
Exponential, SNR=100
Triangle, SNR=100
Box, SNR=100

Figure 3

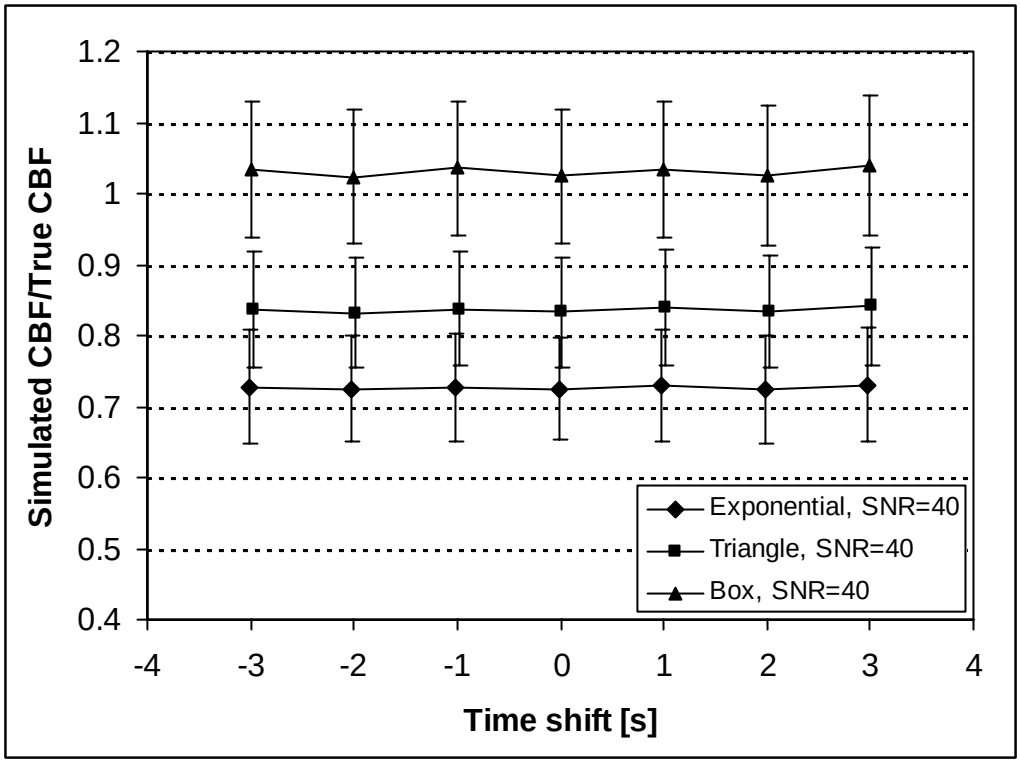
Simulated CBF/True CBF
1.2
1.1
1
0.9
0.8
0.7
0.6
0.5
0.4
-4
-3
-2
-1
0
1
2
3
4
Time shift [s]
Exponential, SNR=40
Triangle, SNR=40
Box, SNR=40

Figure 4